Applied Thermal Engineering 110 (2017) 665–677

Contents lists available at ScienceDirect

Applied Thermal Engineering

journal homepage: www.elsevier.com/locate/apthermeng

Research Paper

Numerical investigation on the combustion characteristics of non-premixed hydrogen-air in a novel micro-combustor

Jiaqiang E [a,b,c,*], Qingguo Peng [a,b,c,*], Xiaohuan Zhao [a,b,c], Wei Zuo [a,b,c], Zhiqing Zhang [b,c], Minhhieu Pham [b,c]

[a] State Key Laboratory of Advanced Design and Manufacturing for Vehicle Body, Hunan University, Changsha 410082, China
[b] College of Mechanical and Vehicle Engineering, Hunan University, Changsha 410082, China
[c] Institute of New Energy and Energy-saving & Emission-reduction Technology, Hunan University, Changsha 410082, China

HIGHLIGHTS

- Proposed a novel micro combustor for non-premixed hydrogen-air combustion.
- Investigated the mixing performance of hydrogen/oxygen in the micro combustor.
- Studied the thermal characteristics and combustion characteristics.
- Obtained the temperature behavior and energy output in the micro combustor.

GRAPHICAL ABSTRACT

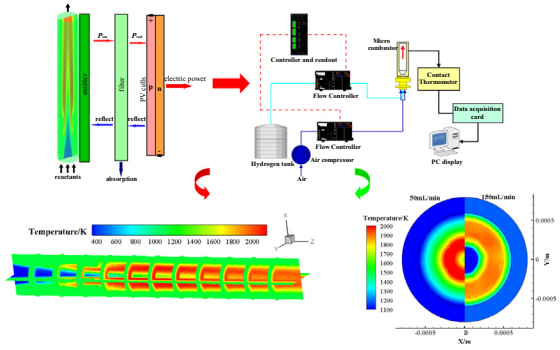

ARTICLE INFO

Article history:
Received 22 May 2016
Revised 1 August 2016
Accepted 30 August 2016
Available online 31 August 2016

Keywords:
Micro combustor
Thermal performance
Cavity
Backward-facing step
Temperature distribution

ABSTRACT

A good mixing of fuel/oxygen is important for the non-premixed combustion in micro combustor, and the thermal performance of outer wall is of significant influence to the application of micro thermo photovoltaic (MTPV) systems. The non-premixed hydrogen/air combustion has been carried out in a novel micro combustor, in addition, the mixing performance of hydrogen/oxygen, the combustion characteristics, working performance of micro combustors are also investigated. Results show that the mixing performance of hydrogen/oxygen can be improved by the adoption of four pipes in combustor, and the thermal performance of combustor affects flame velocity, reaction rate and combustion efficiency. Moreover, the cavity or backward-facing step contributes to the heat recirculation and the flame stabilization, and a high and uniform outer wall temperature distribution is desirable for the application of MTPV system, which can be obtained at the hydrogen volume flow rate 90 mL/min and the equivalence ratio 1.0.

1. Introduction

The micro-power system is developing rapidly depends on that of micro electro mechanical systems (MEMS), various small devices and systems have been successively appearing in human life [1–3]. As a new technology, the micro-power system with features of small dimension, high rate of heat loss and the combustion more unstable compare with macro burning [4,5]. In recent years, many prototypes of micro power devices have been investigated such as micro gas turbines, micro fuel cells and micro thermo photovoltaic (MTPV) systems [6,7].

Investigations on micro combustion, scholars are more likely focus on the combustion characteristics [8]. E et al. [9] numerically studied the effects of inlet velocities, equivalence ratios and bluff

* Corresponding authors at: State Key Laboratory of Advanced Design and Manufacturing for Vehicle Body, Hunan University, Changsha 410082, China.
E-mail addresses: ejiaqiang@126.com (J. E), pengqingguo317@163.com (Q. Peng).

http://dx.doi.org/10.1016/j.applthermaleng.2016.08.210
1359-4311/

Nomenclature

A_i	the flow area, m^2
A_t	the cross-sectional flow area, m^2
a	the thermal diffusivity
d_q	the quenching distance, mm
E	the activation energy of hydrogen combustion reaction, J/mol
$F_{h,j}$	the energy flux of the x_j direction, W
f_{avg}	the ratio of the flow rate of the fuel and total flow
f_i	the mass fraction of the flow
h	the enthalpy of the gas composition, J/kg
h_w	the convective heat transfer coefficient, $W/(m^2\ K)$
$J_{l,j}$	the diffusion flux of species l in the x_j direction, $kmol/(m^2\ s)$
M_l	the molar mass of species l
m_l	the mass fraction of species l
$\dot{m}_{air}$	the air mass flow rate, kg/s
$\dot{m}_{H_2,in}$	the mass flow rate of inlet hydrogen, kg/s
$\dot{m}_{H_2,out}$	the mass flow rate of outlet hydrogen, kg/s
p	the pressure, Pa
p_E	the pressure energy, J/m^3
Q_o	the heat dissipating capacity of the outer wall, W
Q_{Lhv}	the hydrogen lower heating value,119.96 MJ/kg
R	the molar gas constant, J/(mol K)
R_0	the universal gas constant, J/(kmol K)
R_l	the production rate of species l by chemical reaction, $kmol/(m^3\ s)$
S_l	the flame velocity, m/s
T_0	the ambient temperature, K
T_m	the maximum temperature of burned gas, K
T_i	the ignition temperature, K
$T_{w,o}$	the temperature of the outside wall, K
T_∞	the ambient temperature, K
u_i	the velocity component of x_i direction, m/s
u_j	the velocity component of x_j direction, m/s
$v^2/(2g)$	the kinetic energy, J/m^3
$\dot{v}_{H_2}$	the hydrogen volume flow rate, mL/min
w	the inner diameter of combustor, mm

Greek letters

Φ	the equivalence ratio
β	the unmixedness
γ	the energy efficiency
δ	the relative unmixedness
ε	the emissivity of the wall
η	the combustion efficiency
θ	the correction coefficient of the kinetic energy, $\theta = 1.05–1.10$
λ_w	the wall thermal conductivity, W/(m K)
ρ	the gas density, kg/m^3
ρgz	the gravitational potential energy, J/m^3
σ	the Stephan-Boltzman constant, $5.67 \times 10^{-8}\ W\ m^2/K^4$
τ_{ij}	the stress tensor, N

body's blockage ratios on the temperature field, pressure of the combustor wall, combustion efficiency and blow-off limit. Lee et al. [10] studied combustion characteristics of premixed H_2-air micro-flames on a micro-tube. Choi et al. [11] investigated the turbulent mixing characteristics in a micro can type combustor which was promoted by complex flow fields caused by the jet flows and large vortical flow regions. Hosseini and Wahid [12] solved three-dimensional governing equations to investigate the characteristics of lean premixed conventional micro-combustion and lean non-premixed flameless regime of methane/air. Karagiannaki et al. [13] investigated some of the differences and similarities between fully-premixed and stratified lean propane flames stabilized in an axisymmetric bluff-body swirl burner configuration. Yan et al. [14] studied the hydrogen assisted catalytic combustion of methane on platinum, which predicted the effects of changes of hydrogen fraction. Nemitallah et al. [15] investigated an atmospheric diffusion oxy-combustion flame in a gas turbine model combustor, and oxy-combustion and emission characterization, flame stabilization and oxy-combustion model validation analyses were studied. Tang et al. [16] analyzed the combustion characteristics with the differences in flame stabilization, temperature distribution of external wall and flammable channel-heights. Lu et al. [17] found that the combustor performance can be commonly promoted in the hetero-/homogeneous combustion system due to the existence of catalysis. Chen et al. [18] studied the hetero-/homogeneous combustion characteristics and flame stability of lean premixed propane–air mixtures over platinum in micro-combustors, and elucidated the effects of wall thermal conductivity, combustor dimension, flow rate and equivalence ratio on flame stability and combustion efficiency.

Thermal performance and flame stability in combustor are also regarded as immediate areas of research focus [19]. Hossain and Nakamura [20] studied the thermal the diffusion flame via excess heat recirculation through the burner wall of a micro burner. Li et al. [21] analyzed the heat transport of fuel property in terms of the kinetics in the cylindrical micro combustors. Som and Rana [22] made theoretical studies on heat transfer and exergy analysis off low through a narrow tube with heat recirculating wall and embedded thin heat source. Thermal performance is of significant influence to micro combustion, the wall thermal conductivity affect the combustion efficiency of lean H_2/air flame [23], in addition, Hsueh et al. [24] optimized the methanol conversion of the micro-reformer with the serpentine flow field and the combustor with the serpentine flow field via improved thermal management. Micro combustors have high rate of heat loss, Benedetto et al. [25] investigated the heat losses toward the external environment and transverse diffusion which respect to the residence time and significantly affect the thermal behavior of micro combustors, while Wang et al. [26] investigated the surface heat loss with different temperature external winds. Stazio et al. [27] observed three distinct flame behaviors in a micro tubular channel with an external heating which provided by three hydrogen/oxygen flames positioned at the downstream side of the tube. Heat recirculation is of vital importance to micro/meso-scale combustion [28]. Vijayan [29] investigated the effect of recirculation on the wall temperature and the overall energy conversion efficiency. Bagheri and Hosseini [30] investigated flame stability and thermal performance of two different heat recirculation micro-combustors. Lei et al. [31] proposed an annular micro combustion tube with recirculation of exhaust heat and explored the feasibility of combustion in the micro annular tube. Furthermore, Vijayan et al. [32] applied different recirculation methods to improve wall temperature and combustion limits of the micro-scale system. Kedia and Ghoniem [33] found that the laminar premixed flame anchoring near a heat-conducting bluff-body in a micro-combustor with the steel bluff-body. Li et al. [34] added porous medium to a free flame

micro-combustor is able to enhance thermal energy transport, thus allowing more heat recirculation.

In order to obtain a high and uniform wall temperature distribution some structural designs were introduced to combustor [35,36]. Using the micro-combustor with step or bluff body is a useful measure to reduce the gas flow rate locally, which is widely used in studies of micro combustion [37–39]. Baigmohammadi et al. [40] modified and improved of CH_4/air pre-mixed flame in a micro-stepped tube combustor. Yang et al. [41] conducted numerical simulation and experimental test to study the combustion of hydrogen–air mixture in a micro-cylindrical combustor with and without a heat recuperator. Niu et al. [42] investigated the effects of five trapezoidal bluff bodies on blow out limit of methane/air combustion in a micro-channel. Lee et al. [43] and Fan et al. [44] researched on the bluff-body stabilized flames. Other methods also applied to the flame stabilities in micro combustor, Wan et al. [45,46] investigated the flame-anchoring mechanisms of H_2/air flame in channel with cavity. Ran et al. [47] investigated catalytic combustion characteristics of methane in micro-channels with a concave and convex cavity. Li et al. [48] took the porous medium to enhance heat transfer and flame stabilities.

Some new type micro-combustors were designed for the application of MTPV systems. Hua et al. [49] studied the combustion of premixed hydrogen–air mixture in a series of chambers with the same shape aspect ratio under various dimensions from the millimetre to the micron level. Tang et al. [50] designed a new type of micro-combustor for the micro thermo photovoltaic system. Jejurkar and Mishra [51] designed a hollow nitrogen-filled tube inserted in the flame to utilize the external thermal recirculation. Jiang et al. [52] designed a micro planar combustor while Lu et al. [53] built a rectangular micro-combustor. Tang et al. [54] and Su et al. [55] designed multiple-channel micro combustors. As for the non-premixed fuel/air combustion in micro combustor, Ziani and Chaker [56] devoted to the study of the effect of ambient pressure on non-premixed turbulent combustion of a mixture of 20% of hydrogen and 80% of methane. Liu et al. [57] mixings of methane and oxygen in Y-shaped meso-scale combustors with and without porous media were compared numerically. Kim and Park [58] investigated the reacting flows in a CH_4–air micro can combustor with a baffle plate of seven holes.

These literatures reveal that the significance of thermal performance and flame stability to the performance of micro combustor, some useful structural designs and methods were introduced to combustor. However, little researches on non-premixed fuel/air combustion or the couple of cavity and backward-facing step have been reported. The present study seeks to replenish it, and provides some useful information for the design and operation of micro combustor. Furthermore, it contributes to understand the non-premixed hydrogen/air combustion characteristic.

2. Mathematical-physical model of combustion

2.1. Physical model of micro-combustor

In this work, a novel micro combustor is designed, which combines cavity and backward-facing step as shown in Fig. 1. The dimensions of the micro-combustor are 12 mm in length and 1.6 mm in diameter. The micro combustor is established with four pipes named as the suction pipe A, the mixing pipe B, the diffuser pipe C and the shrinkage pipe D. Hydrogen enters into the micro combustor through the circular channel which is of inlet diameter 0.2 mm, while air via the annular channel which is inner diameter 0.6 mm and outer diameter 0.862 mm, and the air inlet has the same area with the hydrogen inlet. In addition, the centerline y = 0 mm and the polyline l_o which is deviated from the wall 0.05 mm.

The suction pipe A is shrink-shaped which provides gradient velocities of air and hydrogen toward the centerline by the lean outer wall and inner wall. The mixing pipe B is for the mixing of oxygen and air, while the diffuser pipe C is set up to make dynamic pressure partly transform into static pressure which increases the pressure difference and the suction efficiency is improved by the diffuser pipe C, in addition, the shrinkage pipe D can prevent tempering. The effectively coupled of these pipes and the thermal transmission (as the red[1] arrows shown in Fig. 1) can improve stable combustion and enhance the reactivity in the micro combustor.

Reactants are burning in the combustor, and then the burned gas will be expelled out via the outlet as shown in Fig. 2 [31,38]. The micro combustor, emitter, filter and PV cells constitute the MTPV system. The original energy of the system is supplied by the micro combustor which acted as an emitter for the micro size. The filter partially absorbs the energy from emitter and transfers to the PV cells which put out electric power via PN junctions, thereby, power is put out for the MTPV system.

2.2. Mathematical description of mathematical-physical model

In the numerical simulation of combustion in the micro combustor, the hydrogen is assumed as the fuel with high power density, longevity, small volume and light weight. The gaseous reactants can be regarded as a continuum and described by Navier–Stokes equations [23,39]. Moreover, the hydrogen mass flow rate and the air mass flow rate are small the maximal, the effects of the fluid volume force and the dissipative can be neglected, in addition, Reynolds number of the gas in the micro combustor is around 200. Hence, the equations for the continuity equation, the momentum conservation equation, the species equation and the energy conservation equation are adopted for this simulation, expressed as follows [47].

The continuity equation:

$$\frac{\partial}{\partial x_i}(\rho u_i) = 0 \tag{1}$$

where ρ is the gas density, kg/m^3; u_i is the velocity component of x_i direction, m/s (i = 1, 2, 3).

The momentum equation:

$$\frac{\partial}{\partial x_j}(\rho u_i u_j - \tau_{ij}) = -\frac{\partial p}{\partial x_i} \tag{2}$$

where p is the pressure, Pa; τ_{ij} is the stress tensor, N; u_j is the velocity component of x_j direction, m/s (j = 1, 2, 3).

The species equation:

$$\frac{\partial}{\partial x_j}(\rho u_j m_l + J_{l,j}) = R_l \tag{3}$$

where m_l is the mass fraction of species l, $J_{l,j}$ is the diffusion flux of species l in the x_j direction, kmol/(m^2 s); R_l is the production rate of species l by chemical reaction, kmol/(m^3 s).

The energy equation:

$$\frac{\partial}{\partial x_j}(\rho u_j h + F_{h,j}) = u_j \frac{\partial p}{\partial x_j} + \tau_{ij}\frac{\partial u_i}{\partial x_j} \tag{4}$$

where h is the enthalpy of gas composition, J/kg; $F_{h,j}$ is the energy flux of the x_j direction, W.

[1] For interpretation of color in Fig. 1, the reader is referred to the web version of this article.

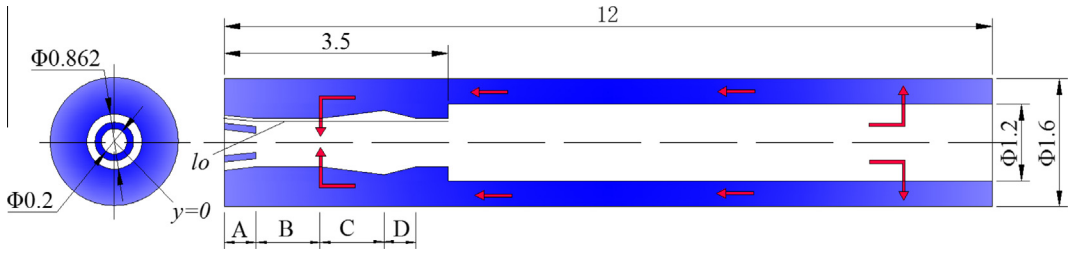

Fig. 1. Geometries of the micro combustor (unit mm).

The energy conservation equation of wall:

$$\frac{\partial(\lambda_w \partial T)}{\partial x_i^2} = 0 \tag{5}$$

where λ_w is the wall thermal conductivity, W/(m K).

The ideal gas equation:

$$p = \rho R_0 T \sum \frac{m_l}{M_l} \tag{6}$$

where R_0 is the universal gas constant, J/(kmol K); M_l is the molar mass of species l.

2.3. Calculation method and model validation

Due to the low mass flow rate of reactants, a three-dimensional, steady state and laminar finite-rate model is adopted for this simulation. The inlet boundary conditions are set as mass flow rate for hydrogen and air, while the outlet boundary condition is pressure outlet. The initial temperature and pressure are 298 K and 0 Pa, respectively. Zero diffusive flux species and no slip boundary conditions are employed at the gas–solid interfaces. Wall of the micro combustor is Silicon. The convection and radiation heat transfer with the environment are coupled, and the convective heat transfer coefficient is 20 W/(m^2 K) and the wall emissivity is set a value of 0.9 [41].

A uniform 3D grid is developed to predict the combustion and the heat transport in the micro combustor. The grid independent test is made by changing the number of elements to the finer elements. For the case hydrogen mass flow rate 1.347 × 10^{-7} kg/s and equivalence ratio is equal to 1.0, as presented in Fig. 3. Three medium meshes with 121,311, 199,239 and 387,588 cells are obtained to observe the changes in the results. Obviously, the mesh with 121,311 cells is of the highest centerline temperature while the mesh of 387,588 cells has the lowest centerline temperature, in addition, the temperature difference for the three radial outlet temperature curves is small. Hence, in order to obtain a better accuracy and saving computation time, the medium mesh with 199,239 cells is more proper for the numerical investigation.

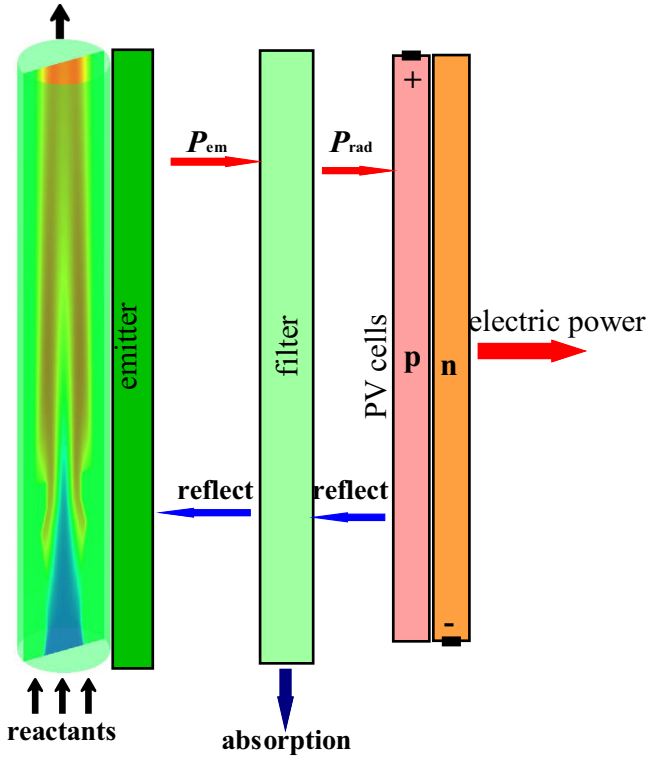

Fig. 2. Schematic of a MTPV system.

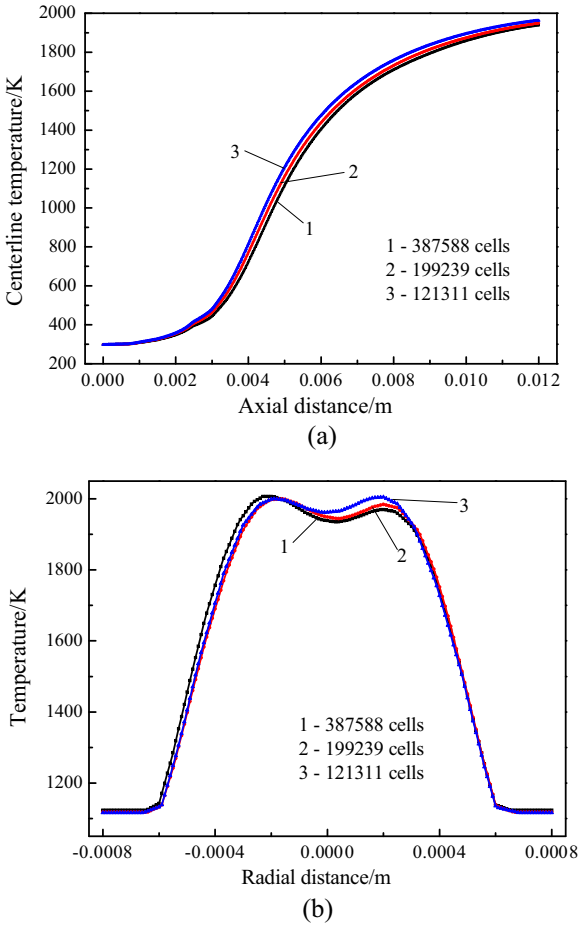

Fig. 3. (a) Axial and (b) radial temperature profile of simulation (at x = 0.012 m from the inlet).

3. Results and discussion

3.1. Experimental verification

To verify the accuracy of the numerical solution, the outer wall temperature of the micro combustor is compared with experiment. In the experiment, the air is supplied via the air compressor while hydrogen enters into the micro combustor from the hydrogen tank. As shown in Fig. 4, the mass flow rates of hydrogen and air are controlled by two SEVENSTAR D07-7B flow controllers which connected with the controller and readout. The hydrogen mass flow rate is 1.347×10^{-7} kg/s and the oxygen mass flow rate is 4.632×10^{-6} kg/s in the experiment. The micro combustor is installed in the experimental bench, a K-type thermocouple is employed to measure the temperature of outer wall by contacted measurement, and the measuring points are located at 2, 5, 8, 10 mm of the micro combustor.

The performance of experiment is presented and compared with the numerical predictions in Fig. 5. The continuous line is obtained from simulation of the case hydrogen inlet mass flow rate 1.347×10^{-7} kg/s (hydrogen volume flow rate 90 mL/min) and equivalence ratio 1.0. It is observed that the deviation between experimental and numerical results is less than 1.42%, which is caused by the measurement accuracy error and the experimental error. Hence, the numerical simulation results are in agreement with the experiment.

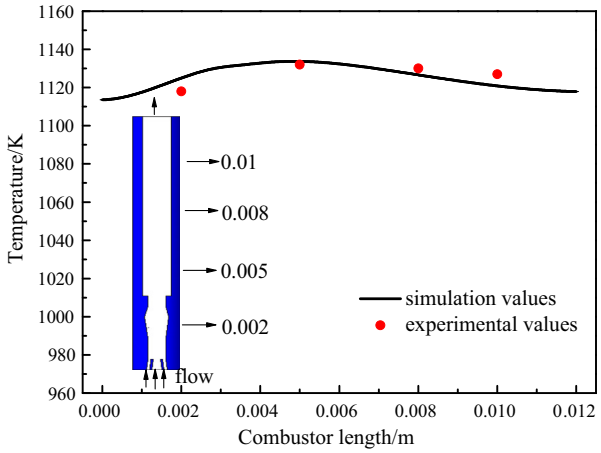

Fig. 5. Comparison of outer wall temperatures between simulation values and experimental values.

Table 1
Inlet flow rates in the micro combustor.

$\dot{v}_{H_2}$ (mL/min)	$\dot{m}_{H_2,in}$ (kg/s)	$\dot{m}_{air}$ (kg/s)
50	7.483×10^{-8}	2.573×10^{-6}
70	1.047×10^{-7}	3.602×10^{-6}
90	1.347×10^{-7}	4.632×10^{-6}
110	1.646×10^{-7}	5.661×10^{-6}
130	1.946×10^{-7}	6.690×10^{-6}
150	2.095×10^{-7}	7.205×10^{-6}

3.2. Mixing performance of hydrogen/oxygen

3.2.1. Pressure and velocity

In this section, effects of four pipes on pressure and velocity in the micro combustor are firstly. To simplify the discussion in this paper the hydrogen volume flow rate value is taken to express hydrogen flow rate, which links with the respective hydrogen volume flow rate and to hydrogen mass flow rate as shown in Table 1. And Table 1 also gives the values of air inlet mass flow rate with the equivalence ratio $\varphi = 1.0$ accordingly.

Figs. 6 and 7 show the distributions of axial pressure and velocity at polyline l_o and line $y = 0$ m (as shown in Fig. 2) for different hydrogen volume flow rates under non-reacting condition, respectively. As shown in Fig. 6, the pressure is decreased with the increase of combustor length for the increase of pipe section area, while the pressure value in mixing pipe B rises firstly and then falls which is caused by the slant inlet and the mixture of reactants. Furthermore, the pressure of high $\dot{v}_{H_2}$ is higher than that of low $\dot{v}_{H_2}$ at the same position in the micro combustor for the effects of boundary. Obviously, the pressure value of polyline l_o is greater than the line $y = 0$ m at the same position.

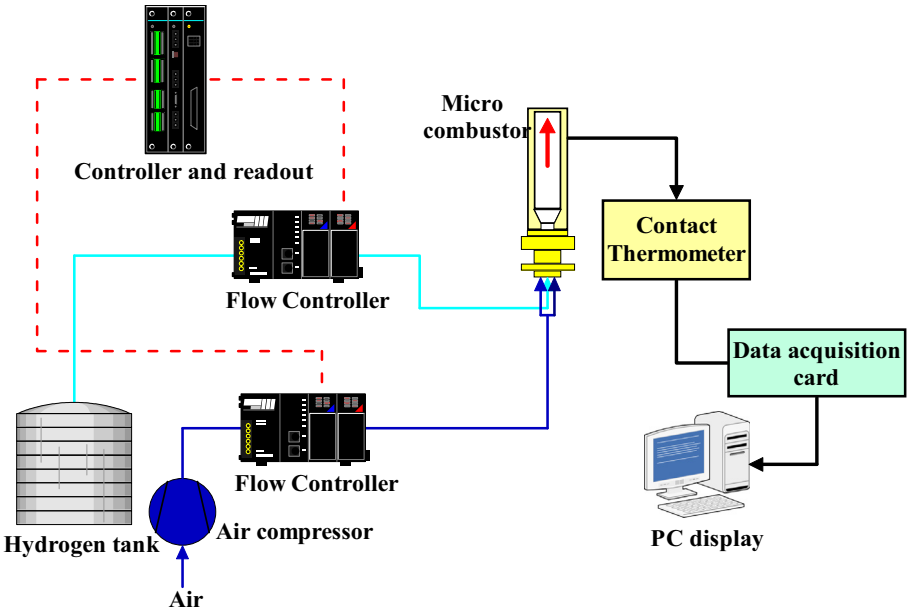

Fig. 4. Schematic of a platform experiment for reaction.

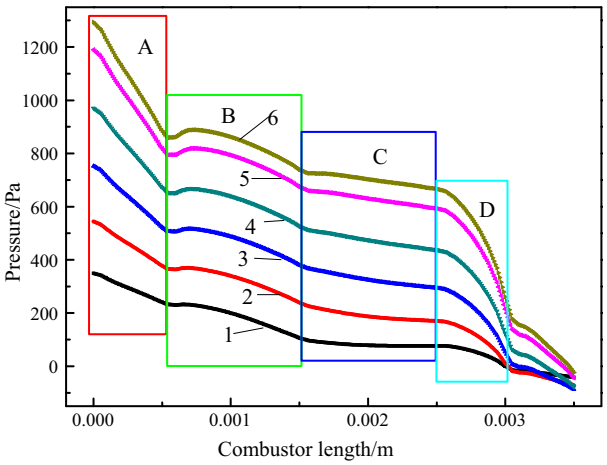

(a) polyline l_o

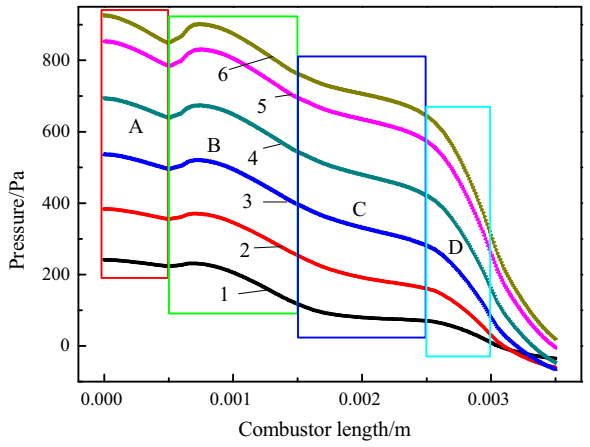

(b) line y=0

1-50mL/min; 2-70mL/min; 3-90mL/min;4-110mL/min;
5-130mL/min;6-150mL/min

Fig. 6. Distributions of axial pressure of the micro combustor for different hydrogen volume flow rates.

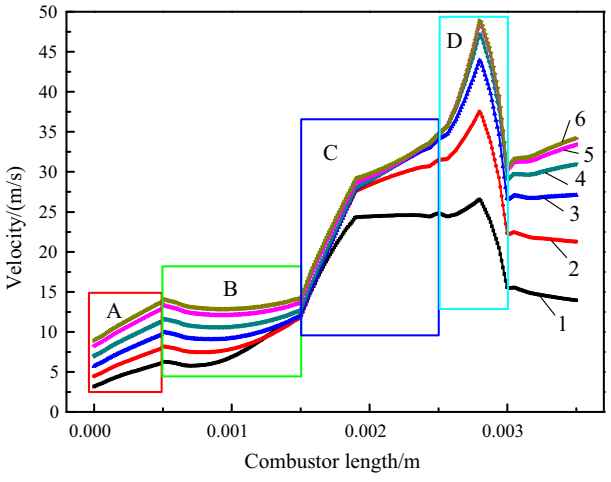

(a) polyline l_o

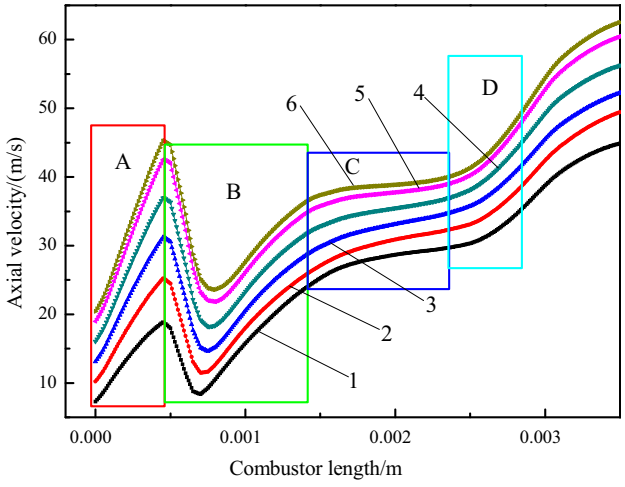

(b) line y=0m

1-50mL/min; 2-70mL/min; 3-90mL/min;
4-110mL/min;5-130mL/min;6-150mL/min

Fig. 7. Distributions of the axial velocity of the micro combustor for different hydrogen volume flow rates.

As shown in Fig. 7, with the increase of $\dot{v}_{H_2}$, the velocity is increased at the same location of combustor. On the whole, the velocity of polyline l_o arises with the increase of combustor length, but there exist two mutations in the mixing pipe B and the shrinkage pipe D, due to the mixture of hydrogen and oxygen in the mixing pipe B and the polyline l_o is close to the cavity which can reduce the velocity of reactants. However, the velocity of line $y = 0$ m arises with the increase of combustor length, except for the mixing pipe B, because the cavity has a very low impact on it.

The Bernoulli equation is expressed as Eq. (7).

$$\rho g z + p_E + \frac{\theta \rho v^2}{2} = \text{const} \tag{7}$$

where ρgz is the gravitational potential energy, J/m^3; p_E is the pressure energy, J/m^3; $v^2/(2g)$ is the kinetic energy, J/m^3; θ is the correction coefficient of the kinetic energy, θ = 1.05–1.10.

As for the axial pressure and velocity, the changing trends of them for different $\dot{v}_{H_2}$ are the same with variations different degree. Fig. 8 indicates the distributions of axial pressure and velocity in the centerline of micro combustor without reaction for the case $\dot{v}_{H_2}$ = 90 mL/min and Φ = 1.0. In the suction pipe A, with increase of combustor length, the pressure which has the

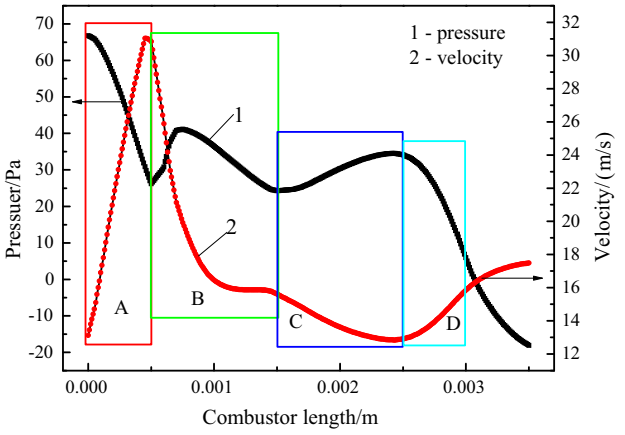

Fig. 8. Distributions of axial pressure and velocity in the centerline of micro combustor without reaction ($\dot{v}_{H_2}$ = 90 mL/min and Φ = 1.0).

peak pressure at the entrance is decreased while the velocity is arose to the peak value. In the mixing pipe B, the axial pressure is firstly increased and then felled, on the contrary, there exists a small amplification after the decreasing amplitude of the velocity. There exists an increase for the pressure while a decrease for the velocity in the diffuser pipe C, but the pressure is decreased and the velocity is increased in the shrinkage pipe D. This is caused by the mutual transformation between potential energy and kinetic energy. Moreover, the total energy of the gas flow remains the same at any cross section in the micro combustor (according to the Bernoulli Eq. (7)), where the flow energy loss is ignored.

3.2.2. Mixedness

Good mixing performance of the fuel and the oxidant can make a sufficiently reaction. It is contribute to the improvement of the combustion efficiency and the output of the MTPV system. The relative unmixedness is introduced to evaluate the mixing performance of hydrogen/air in the micro combustor. When the relative unmixedness is smaller, the mixing performance of the hydrogen/air can be better.

The unmixedness β is expressed as Eq. (8) [59].

$$\beta = \sqrt{\frac{1}{A_t}\sum A_i (f_i - f_{avg})^2} \tag{8}$$

where A_t is the cross-sectional flow area, m^2; A_i is the flow area, m^2; f_i is the mass fraction of the flow; f_{avg} is the ratio of the flow rate of the fuel and total flow.

The relative unmixedness δ is expressed as Eq. (9).

$$\delta = \frac{\beta / f_{avg}}{F} \tag{9}$$

where $F = \sqrt{\frac{1-f_{avg}}{f_{avg}}}$.

The relative unmixedness δ is the dimensionless parameter between 0 and 1. Fig. 9 indicates that the relative unmixedness δ at $z = 1.5$ mm is higher than that of at $z = 2.5$ mm, due to the diffuser pipe C can improve the mixing performance of hydrogen/air. Furthermore, the relative unmixedness δ increases with the increase of $\dot{v}_{H_2}$, which caused by the needs of more hydrogen to be mixed in the micro combustor.

Fig. 10 presents the hydrogen and oxygen mass fraction distributions at planes z = 1.5 mm and z = 2.5 mm of the micro combustor for the case $\Phi = 1.0$ and $\dot{v}_{H_2} = 90$ mL/min under non-reacting condition. The hydrogen mass fraction is low near the wall and high in the center at the location $z = 1.5$ mm and $z = 2.5$ mm, while the oxygen mass fraction is high near the wall and low in the center at $z = 1.5$ mm and $z = 2.5$ mm. Obviously, the mass fraction of hydrogen or oxygen is higher at $z = 1.5$ mm than that of $z = 2.5$ mm, which is consistent with the results in Fig. 9.

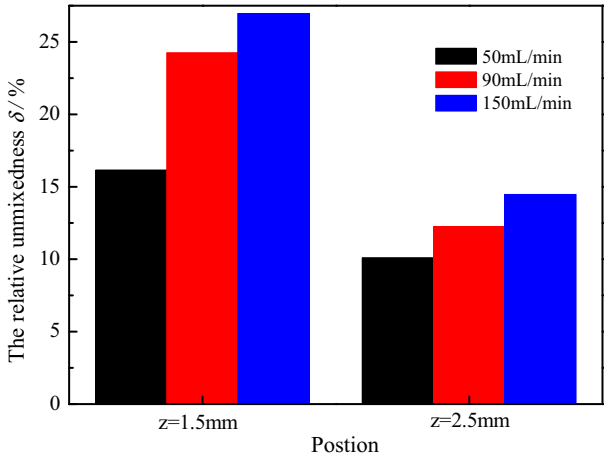

Fig. 9. The relative unmixedness δ at planes $z = 1.5$ mm and $z = 2.5$ mm under the condition of non-reacting and $\Phi = 1.0$.

3.3. Combustion characteristics

3.3.1. Thermal characteristics

Fig. 11 shows the temperature distribution of the case $\Phi = 1.0$ and $\dot{v}_{H_2} = 90$ mL/min. The temperature distribution in fluid region of the micro combustor can be mainly divided into three zones: (1) the inlet zone which has lower temperature, (2) the flame zone that is the highest temperature in the combustion chamber, (3) the outlet that is also a high temperature zone. The inlet zone is preheated by the heat from the flame zone and the outlet zone (as shown in Fig. 1), which can improve the initial temperature of reactants.

Flame velocity S_l in combustor related to many factors, as follows:

$$S_l \propto \sqrt{a\left(\frac{w - 2d_q}{w}\right)\left(\frac{T_m - T_i}{T_i - T_0}\right) \cdot p^{n-1} \cdot \exp\left(-\frac{E}{RT_m}\right)} \tag{10}$$

where a is the thermal diffusivity; w is the inner diameter of combustor, mm; d_q is the quenching distance, mm; E is the activation energy of hydrogen combustion reaction, J/mol; R is the molar gas constant, J/(mol K); T_i is the ignition temperature, K; T_m is the maximum temperature of burned gas, K; T_0 is the upstream temperature for infinite point, K.

Formula (10) indicates that the flame velocity is not only proportional to the square root of a and the chemical reaction rate, but also related to d_q. In the macro scale combustor, w is much larger than the d_q and $(w - d_q)/w \approx 1$, thus, d_q can be ignored. However, the change of d_q affects relatively more on $(w - d_q)/w$ in micro combustor, and d_q has a greater impact on S_l. As shown in Fig. 12, the cavity (composed of diffuser pipe C and shrinkage pipe D) or the backward-facing step in the combustor leads to a higher value of $(w - d_q)/w$, it will make the increase of flame velocity.

The schematic of the flow field in Fig. 12 also outlines that the high-temperature reflow zone formed in the cavity at the case $\dot{v}_{H_2} = 50$ mL/min and $\Phi = 1.0$ while the case $\dot{v}_{H_2} = 150$ mL/min and $\Phi = 1.0$ located behind the backward-facing step. Moreover, the reflow zone behind the backward-facing step at $\dot{v}_{H_2} = 150$ mL/min is larger than $\dot{v}_{H_2} = 50$ mL/min, which means that the backward-facing step plays a greater influence at high $\dot{v}_{H_2}$. Therefore, part of the high-temperature gas flows back to the flame root, and igniting the reactants at upstream continuously, in this way, the combustion in the micro combustor can be stabilized.

To study the thermal characteristics of the micro combustor ulteriorly, the temperature comparison of cross sections at z = 4 mm in the case $\dot{v}_{H_2} = 50$ mL/min and $\dot{v}_{H_2} = 150$ mL/min under the condition of 1.0 is shown in Fig. 13. The wall temperature of $\dot{v}_{H_2} = 150$ mL/min is higher than that of $\dot{v}_{H_2} = 50$ mL/min, but the center zone in the combustion chamber of $\dot{v}_{H_2} = 50$ mL/min is higher than $\dot{v}_{H_2} = 150$ mL/min. Furthermore, the temperature distribution in the combustion chamber is doughnut-shape, and it is low around the centerline or near the wall and high in the middle region.

3.3.2. Reaction rate and combustion efficiency

Fig. 14 provides the reaction rate of the center plane in the micro combustor under the condition of $\Phi = 1.0$. In this figure, the reaction zone is defined according to the change in reaction rate [30]. It can be clearly seen that the reaction zone of high hydrogen volume flow rate $\dot{v}_{H_2}$ is bigger than that of low $\dot{v}_{H_2}$, but

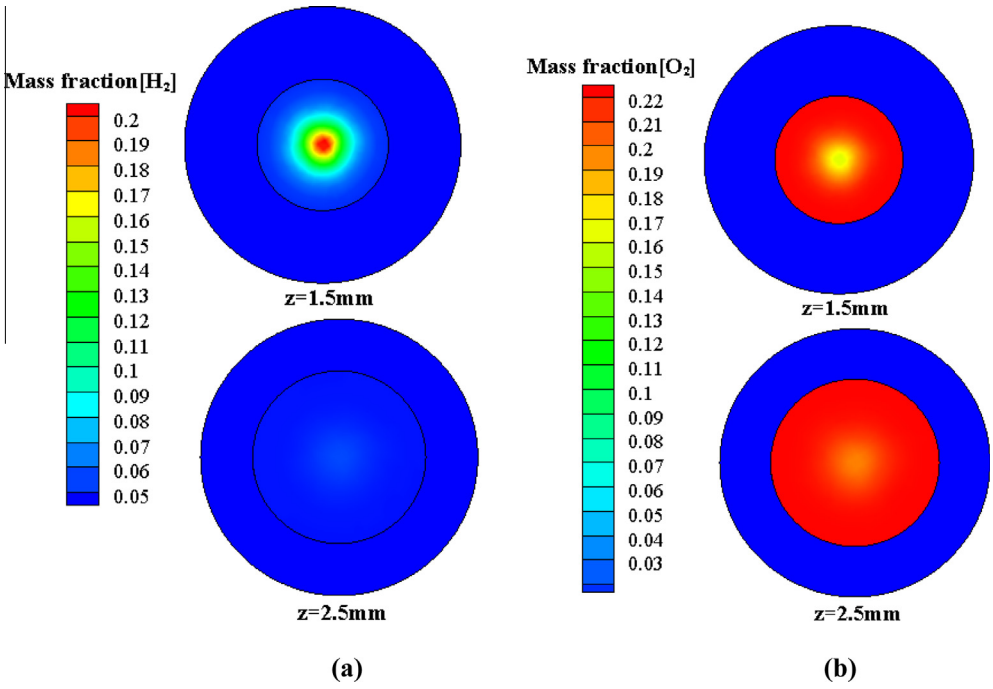

Fig. 10. Hydrogen (a) and oxygen (b) mass fraction distributions at planes z = 1.5 mm and z = 2.5 mm for the case Φ = 1.0 and $\dot{v}_{H_2}$ = 90 mL/min under non-reacting condition.

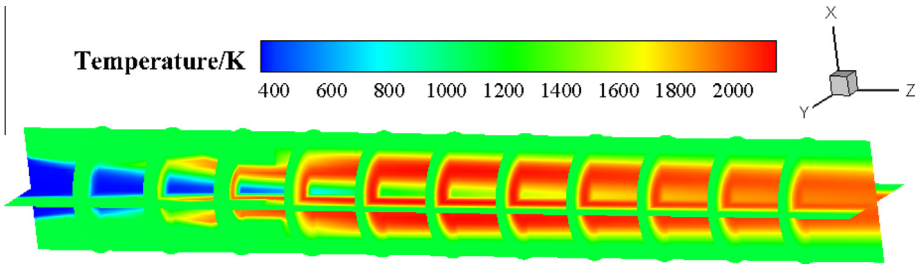

Fig. 11. Temperature distribution of the case Φ = 1.0 and $\dot{v}_{H_2}$ = 90 mL/min.

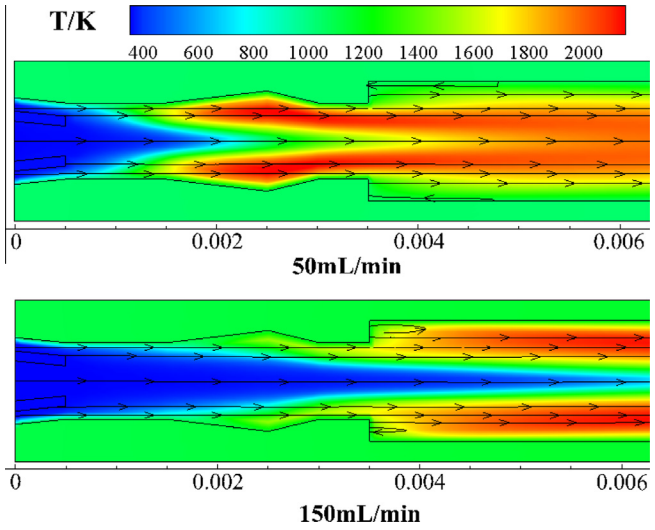

Fig. 12. Schematic of the flow field in the micro combustor for Φ = 1.0 (coloring by temperature). (For interpretation of the references to color in this figure legend, the reader is referred to the web version of this article.)

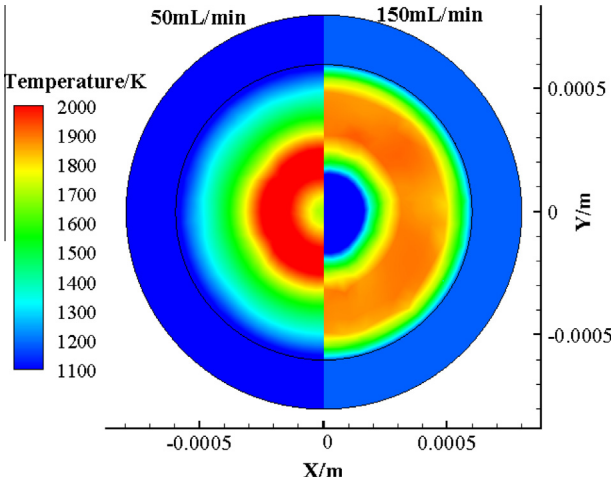

Fig. 13. Temperature comparison of cross sections at z = 4 mm in the case $\dot{v}_{H_2}$ = 50 mL/min and $\dot{v}_{H_2}$ = 150 mL/min under the condition of Φ = 1.0.

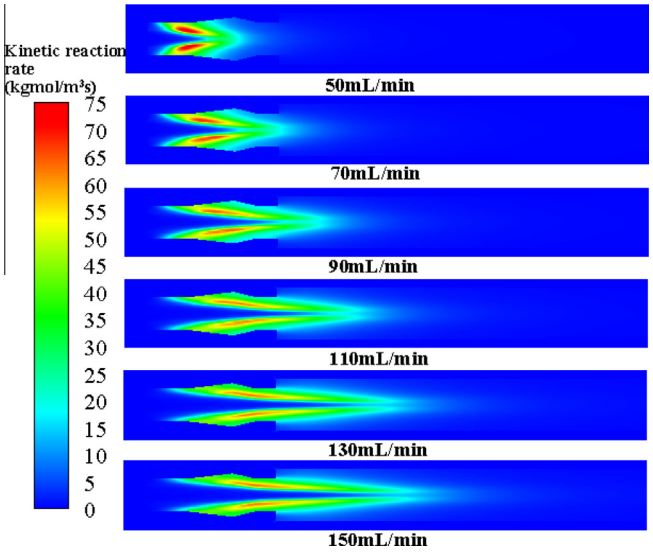

Fig. 14. Center plane reaction rate for different hydrogen flow rate under the condition of $\Phi = 1.0$.

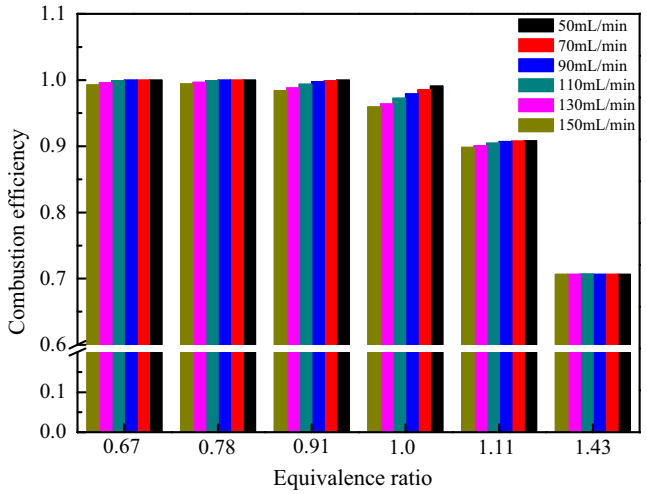

Fig. 15. Effects of equivalence ratio on combustion efficiency for different hydrogen volume flow rates.

the reaction rate of low $\dot{v}_{H_2}$ is higher than that of high $\dot{v}_{H_2}$. It is observed that the location of the reaction zone is affected by the preheating of reactants which exerts a dominant effect. It is apparent that the heat need for preheating (from combustion gas to reactive flow for low) at low $\dot{v}_{H_2}$ is considerably lesser than that of high $\dot{v}_{H_2}$. Hence, reactants heat up faster and the reaction zone stretch closer to the inlet [30]. Therefore, it can be expounded that the bigger reaction zone at high $\dot{v}_{H_2}$ is in agreement with a bigger flame thickness (or a lager high temperature zone) and the higher reaction rate at low $\dot{v}_{H_2}$ is in agreement with a higher flame velocity (according to Eq. (10)).

Combustion efficiency affects the performance of combustor [18,23]. For hydrogen is the only fuel in this study, the combustion efficiency η can be represented by the hydrogen mass consume.

$$\eta = \frac{\dot{m}_{H_2,in} - \dot{m}_{H_2,out}}{\dot{m}_{H_2,in}} \tag{11}$$

where $\dot{m}_{H_2,in}$ is the mass flow rate of inlet hydrogen, kg/s; $\dot{m}_{H_2,out}$ stands for the mass flow rate of outlet hydrogen, kg/s.

Fig. 15 shows the effects of equivalence ratio on combustion efficiency under various $\dot{v}_{H_2}$. The combustion efficiency η increases with the increase of the equivalence ratio Φ, in addition, η is exceed 0.95 at $\Phi \leqslant 1.0$, due to more air is provided at low Φ and the mixing performance is better, therefore, the reaction of oxygen/hydrogen is more fully. When Φ is higher than 1.0, η is lower for the shortage of oxygen in reaction. Furthermore, η has a little reduction with the increase of $\dot{v}_{H_2}$, due to the Arrhenius factor and its sensitive dependence for the larger value of preheating temperature [21], the residence time of reactants in the combustion chamber shortens with increase of $\dot{v}_{H_2}$, and more hydrogen is blown out the combustion chamber before burning for a higher velocity of hydrogen/air at high $\dot{v}_{H_2}$.

Fig. 16 shows that the effects of the inlet pressure on η under the condition of $\Phi = 1.0$ and $\dot{v}_{H_2} = 90$ mL/min, where the inlet pressures of hydrogen and air take the same value. η has a volatility with the increase of the inlet pressure, but the volatility is small and the biggest amplification is 0.02386% at the inlet pressure 0.06 MPa while the maximum decreasing amplitude is 0.01881% at 0.11 MPa. This phenomenon can originate in two factors. Firstly, the reaction rate decreases with the increase of inlet pressure, which leads to a lower heat release rate [46]. Secondly, more

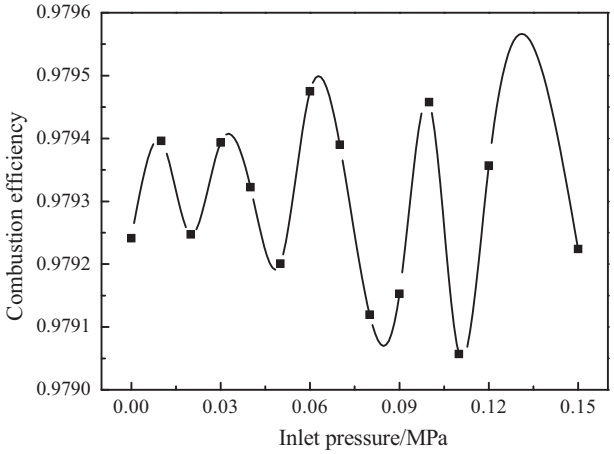

Fig. 16. Effects of inlet pressure on combustion efficiency under the condition of $\Phi = 1.0$ and $\dot{v}_{H_2} = 90$ mL/min.

reactants are exhausted out of before receiving sufficiently preheating energy and beginning to burn. Thereby, the effects on the inlet pressure is insignificant at $\Phi = 1.0$ and $\dot{v}_{H_2} = 90$ mL/min.

3.3.3. Temperature distribution and flame

Fig. 13 indicates that the high temperature region is different for various hydrogen volume flow rate $\dot{v}_{H_2}$. In order to investigate the combustion characteristic of the micro combustor, the temperature distributions of the micro combustor in the center plane is shown in Fig. 17. The temperature of flame center (the high temperature region) increases with the increase of $\dot{v}_{H_2}$. A reasonable explanation for the phenomenon is that the preheating of reactants has significant influence on residence time, which is prolonged with the increase of inlet velocity [25], while the temperature difference between the fluid and the wall is small in the combustion chamber and the heat convection for them is weak at low $\dot{v}_{H_2}$ (as shown in Fig. 13). With the gradual increase of $\dot{v}_{H_2}$ or equivalence ratio Φ, the convective heat gradually grown and then the flame temperature is boosted. Furthermore, $\Phi = 0.91$, $\Phi = 1.0$ and $\Phi = 1.11$ are more suitable for the application of MTPV for a larger and a higher flame temperature which can provide more energy as shown in Fig. 17(b).

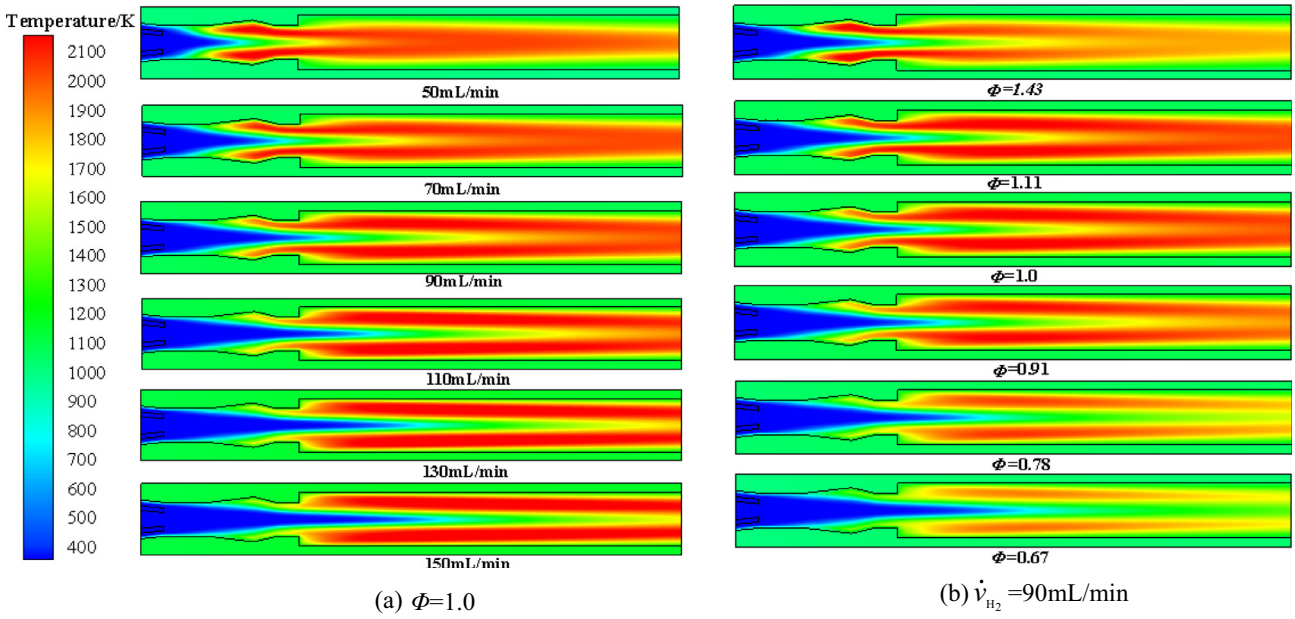

Fig. 17. Temperature distributions of the micro combustor in the center plane. (a) Different hydrogen volume flow rates at $\Phi = 1.0$, (b) different equivalence ratios at $\dot{v}_{H_2} = 90$ mL/min.

Moreover, the flame location will be moved forward with the increase of $\dot{v}_{H_2}$ or the reduce of Φ, in addition, the flame stabilized behind the backward-facing step at high $\dot{v}_{H_2}$ or low Φ, while it stabilized in the cavity at low $\dot{v}_{H_2}$ or high Φ, due to the increased velocity of reactants will cut down the time for the convective heat transfer and reduce the time of preheating, while longer time is required for the preheating of reactants before it reaches the ignition temperature. Obviously, the cavity and the backward-facing step can simultaneously provide a low velocity, better heat recirculation and high-local temperature region, which is the main flame anchoring mechanism of the micro combustor [46,47].

Fig. 18 shows that the effects of hydrogen volume flow rate and equivalence ratio on the centerline temperature distribution, which can be increased along the axial direction from the inlet and reaches a maximum value [18]. The centerline temperature profiles are increased slowly near the entrance, and then they have a rapid increase at location z = 2 mm, z = 3 mm and z = 5 mm for the $\dot{v}_{H_2}$ takes the value of 50, 90 and 150 mL/min, respectively. The reason is that the reaction zone (or the flame location) moved towards downstream, where the gas temperature is increased quickly. However, the combustion heat is transferred rapidly through combustor wall via heat conduction and convective heat transfer [25,29], which leads to much heat loss in the downstream of combustor, in addition, the high-temperature zone is doughnut-shape (seen in Fig. 13) in combustion chamber. The two factors cause that the centerline temperature distributions level off at the downstream of combustor.

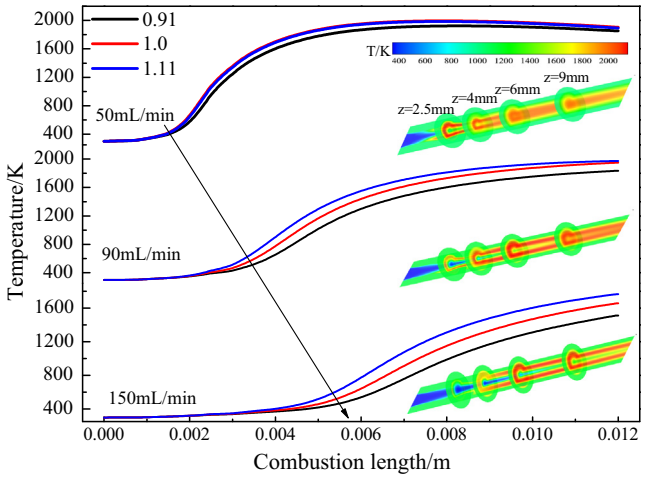

Fig. 18. Centerline temperature distributions of the micro combustor for different hydrogen volume flow rates and equivalence ratios.

Fig. 18 also indicates that with the increase of Φ, the centerline temperature is increased (except for the case $\Phi = 1.11$ and $\dot{v}_{H_2} = 50$ mL/min), due to the flame temperature increases with the increase of Φ (see Fig. 17(b)), while the heat loss of $\dot{v}_{H_2} = 50$ mL/min is larger and it has a higher heat loss rate. Hence, refer to Figs. 17(b) and 18 only consider the temperature distribution in the combustion chamber, it can be concluded that $\Phi = 1.11$ can obtains the highest temperature.

3.4. Outer wall temperature profile and output

A high and uniform wall temperature distribution is desirable for the application of the micro TPV system [50,55]. As Fig. 19 indicates that the temperature of the outer wall surface increases with the increase of the hydrogen volume flow rate $\dot{v}_{H_2}$, where it ranges from 50 mL/min to 150 mL/min under the condition $\Phi = 1.0$, and these temperature curves reach the highest temperature at the intermediate section of combustor. Furthermore, the region of high temperature gradually moves forward to downstream with the increase of $\dot{v}_{H_2}$ which indicated by the arrow in Fig. 19, due to the flame center position moves to the downstream progressively as shown in Fig. 17. Moreover, the uniformity of these temperature curves has a great difference, the outer wall temperature of $\dot{v}_{H_2} = 70$, 90 and 110 mL/min are more uniform, for the temperature variances of them are 54.16 K, 37.13 K and 78.65 K, respectively.

Referring to Figs. 17(b) and 18, it is observed that the equivalence ratio affects the wall temperature distribution. As shown in Fig. 20, when the equivalence ratio takes the value such as $\Phi = 0.91$, $\Phi = 1.0$ and $\Phi = 1.11$ under the condition of $\dot{v}_{H_2} = 90$ mL/min, the temperature distributions of outer wall have higher value and the case $\Phi = 1.0$ is the highest one. Moreover,

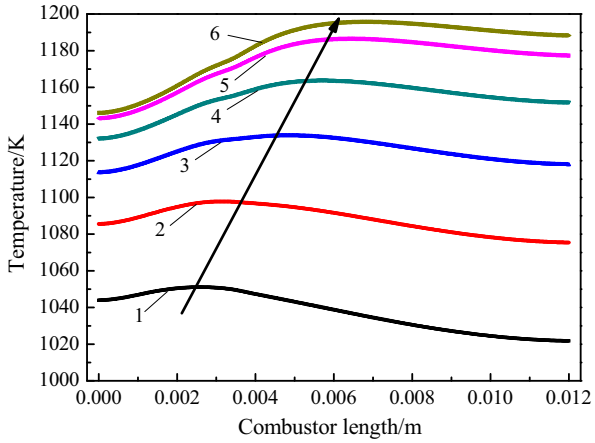

Fig. 19. Distributions of outer wall temperature for different hydrogen volume flow rates under the condition Φ = 1.0.

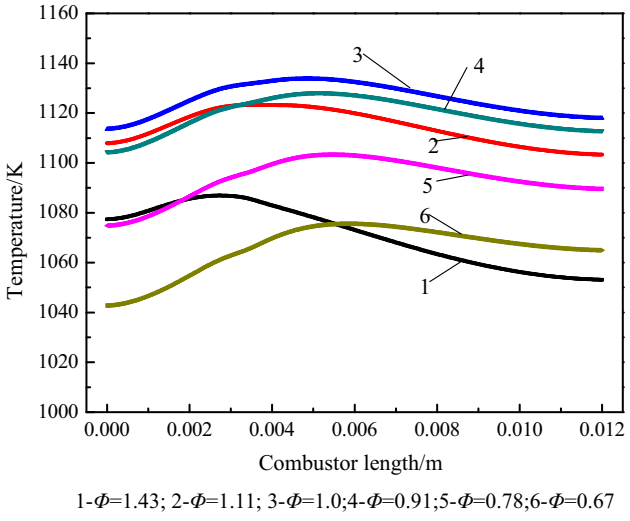

Fig. 20. Distributions of outer wall temperature for different equivalence ratios under the condition of $\dot{v}_{H_2}$ = 90 mL/min.

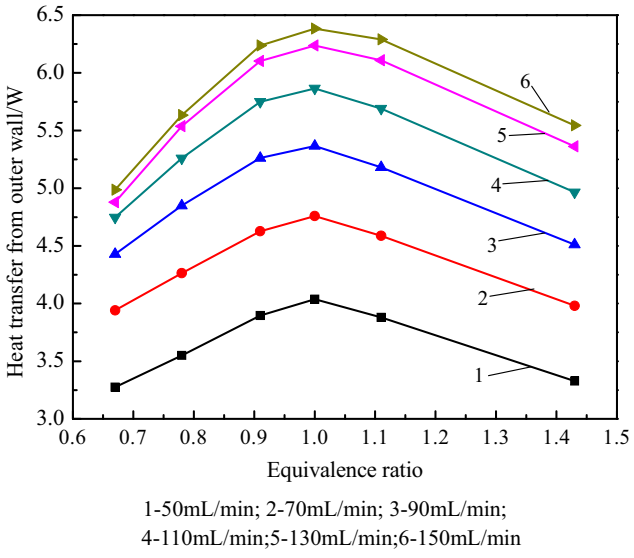

Fig. 21. Effects of equivalence ratio on heat transfer from outer wall for different hydrogen volume flow rates.

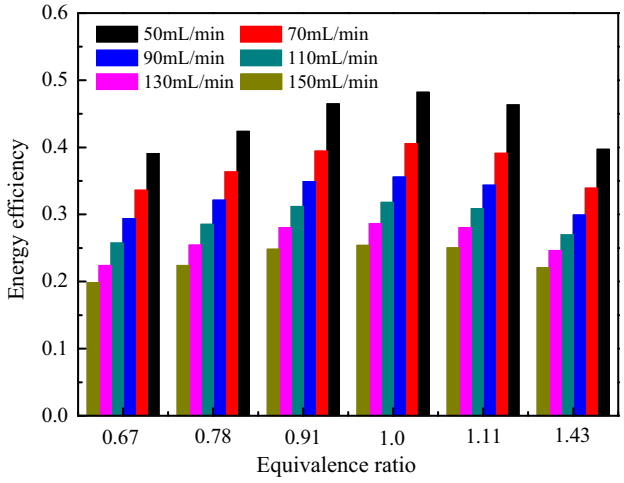

Fig. 22. Effects of equivalence ratio on energy efficiency for different hydrogen volume flow rates.

when the equivalence ratio takes the values of 0.67, 0.78, 0.90, 1.0, 1.11 and 1.43, the temperature variances are 91.38 K, 62.54 K, 44.70 K, 37.13 K, 45.61 K and 137.0 K, respectively. It means that the micro combustor is of the most uniform temperature distribution at Φ = 1.0, which is conducive to the application of the MTPV system.

As Fig. 2 indicates that the energy output of the combustor is very important for the MTPV system, while the energy output of the combustor is combined the radiation heat with the convective heat transfer between the outer wall surface and the ambience. The heat dissipating capacity of the outside wall is Q_o:

$$Q_o = h_w(T_{w,o} - T_\infty) + \varepsilon\sigma\left(T_{w,o}^4 - T_\infty^4\right) \quad (12)$$

where h_w is the convective heat transfer coefficient, W/(m^2 K); $T_{w,o}$ is the temperature of the outside wall, K; T_∞ is the ambient temperature, K; σ is the Stephan-Boltzman constant, 5.67 × 10^{-8} W m^2/K^4; ε is the emissivity of the wall.

According to Eq. (12) the outer wall temperature can decide the energy output of the combustor, while the equivalence ratio Φ and the hydrogen volume flow rate $\dot{v}_{H_2}$ have great influence on it (as shown in Fig. 17). Fig. 21 shows the effects of Φ and $\dot{v}_{H_2}$ on the energy output Q_o, when Φ takes the value ranges from 0.67 to 1.43, Q_o increases first and then falls with the increase of Φ at a fixed value of $\dot{v}_{H_2}$, and the maximum value of Q_o appeared at Φ = 1.0, which caused by the highest outer wall temperature (see Fig. 20). While Q_o increases with the increase of $\dot{v}_{H_2}$ at the same value of Φ, due to the increased reaction energy which makes higher outer wall temperature.

In order to interpret the results of micro combustion, the energy efficiency γ is introduced, which represented as the ratio of the heat transfer from the outer wall Q_o to the heat rate of reaction.

$$\gamma = \frac{Q_0}{\dot{m}_{H2,in} Q_{Lhv}} \quad (13)$$

where Q_{Lhv} is the hydrogen lower heating value which takes a constant value of 119.96 MJ/kg [60].

Fig. 22 indicates that with the increase of the hydrogen volume flow rate $\dot{v}_{H_2}$, the energy efficiency γ is reduced at a fixed value of equivalence ratio Φ, which is caused by a lower combustion

efficiency η and a lower temperature of fluid near the outlet at a lower $\dot{v}_{H_2}$. Furthermore, the energy efficiency γ obtains maximum value at Φ = 1.0 the increases first and then falls with the increase of Φ. Therefore, it can be stated that the energy efficiency γ is in agreement with the energy output Q_o.

4. Conclusions

A numerical study on the non-premixed hydrogen/air combustion is conducted. The main conclusions are summarized as follows:

(1) The mixing performance of hydrogen/oxygen can be improved by the adoption of the suction pipe A, the mixing pipe B, the diffuser pipe C and the shrinkage pipe D in the micro combustor.
(2) Thermal performance is of significant influence to micro combustion, and it affects flame velocity, reaction rate and combustion efficiency in the micro combustor.
(3) The cavity composed of the diffuser pipe C and the shrinkage pipe D and the backward-facing step in the combustor can simultaneously provide a recirculation and low velocity zone, which contribute to the flame stabilization.
(4) The flame temperature increases with the increase of the hydrogen volume flow rate or the equivalence ratio.
(5) A high and uniform outer wall temperature distribution is obtained for the application of MTPV system at the hydrogen volume flow rate 90 mL/min and the equivalence ratio 1.0.

Conflict of interests

The authors declare that they have no conflict of interests regarding the publication of this paper.

Acknowledgements

This work is supported by the National Natural Science Foundation of China (51176045).

References

[1] V. Vijayan, A.K. Gupta, Thermal performance of a meso-scale liquid-fuel combustor, Appl. Energy 88 (7) (2011) 2335–2343.
[2] V. Shirsat, A.K. Gupta, Extinction, discharge, and thrust characteristics of methanol fueled meso-scale thrust chamber, Appl. Energy 103 (2013) 375–392.
[3] Y. Ju, K. Maruta, Microscale combustion: technology development and fundamental research, Prog. Energy Combust. Sci. 37 (2011) 669–715.
[4] J.Q. E, Q.G. Peng, X.L. Liu, W. Zuo, X.H. Zhao, H.L. Liu, Numerical investigation on hydrogen/air non-premixed combustion in a three-dimensional micro combustor, Energy Convers. Manage. 124 (2016) 427–438.
[5] J.Q. E, W. Zuo, X.L. Liu, Q.G. Peng, Y.W. Deng, H. Zhu, Effects of inlet pressure on wall temperature and exergy efficiency of the micro-cylindrical combustor with a step, Appl. Energy 175 (2016) 337–345.
[6] D. Zhao, C. Ji, S. Li, J. Li, Thermodynamic measurement and analysis of dual-temperature thermoacoustic oscillations for energy harvesting application, Energy 65 (2014) 517–526.
[7] J.F. Pan, J. Huang, D.T. Li, W.M. Yang, W.X. Tang, H. Xue, Effects of major parameters on micro-combustion for thermophotovoltaic energy conversion, Appl. Therm. Eng. 27 (2007) 1089–1095.
[8] S. Kikui, T. Kamada, H. Nakamura, T. Tezuka, S. Hasegawa, K. Maruta, Characteristics of n-butane weak flames at elevated pressures in a micro flow reactor with a controlled temperature profile, Proc. Combust. Inst. 35 (2015) 3405–3412.
[9] J.Q. E, H.J. Huang, X.H. Zhao, Numerical investigation on effects of bluff body in flat plate micro thermo photovoltaic combustor with sudden expansion, J. Cent. South Univ. 23 (4) (2016) 975–982.
[10] K.H. Lee, Y.T. Hong, K.B. Kim, O.C. Kwon, Stability limits of premixed microflames at elevated temperatures for portable fuel processing devices, Int. J. Hydrogen Energy 33 (2008) 232–239.
[11] H.S. Choi, T.S. Park, K. Suzuki, Turbulent mixing of a passive scalar in confined multiple jet flows of a micro combustor, Int. J. Heat Mass Transf. 51 (2008) 4276–4286.
[12] S.E. Hosseini, M.A. Wahid, Investigation of Bluff-body micro-flameless combustion, Energy Convers. Manage. 88 (2014) 120–128.
[13] C. Karagiannaki, E. Dogkas, G. Paterakis, K. Souflas, E.Z. Psarakis, P. Vasiliou, P. Koutmos, A comparison of the characteristics of disk stabilized lean propane flames operated under premixed or stratified inlet mixture conditions, Exp. Therm. Fluid Sci. 59 (2014) 264–274.
[14] Y. Yan, W. Tang, L. Zhang, W. Pan, Z. Yang, Y. Chen, J. Lin, Numerical simulation of the effect of hydrogen addition fraction on catalytic micro-combustion characteristics of methane-air, Int. J. Hydrogen Energy 39 (2014) 1864–1873.
[15] M.A. Nemitallah, M.A. Habib, Experimental and numerical investigations of an atmospheric diffusion oxy-combustion flame in a gas turbine model combustor, Appl. Energy 111 (2013) 401–415.
[16] A.K. Tang, Y.M. Xu, C.X. Shan, J.F. Pan, Y.X. Liu, A comparative study on combustion characteristics of methane, propane and hydrogen fuels in a micro-combustor, Int. J. Hydrogen Energy 40 (46) (2015) 16587–16596.
[17] Q.B. Lu, J.F. Pan, W.M. Yang, Z.H. Pan, A.K. Tang, Y. Zhang, Effects of products from heterogeneous reactions on homogeneous combustion for H_2/O_2 mixture in the micro combustor, Appl. Therm. Eng. 102 (2016) 897–903.
[18] J. Chen, W. Song, X. Gao, D. Xu, Hetero-/homogeneous combustion and flame stability of fuel-lean propane-air mixtures over platinum in catalytic micro-combustors, Appl. Therm. Eng. 100 (2016) 932–943.
[19] Y. Yan, W. Tang, L. Zhang, W. Pan, L. Li, Thermal and chemical effects of hydrogen addition on catalytic micro-combustion of methane–air, Int. J. Hydrogen Energy 39 (2014) 19204–19211.
[20] A. Hossain, Y. Nakamura, Thermal and chemical structures formed in the micro burner of miniaturized hydrogen-air jet flames, Proc. Combust. Inst. 35 (2015) 3413–3420.
[21] J. Li, S.K. Chou, Z.W. Li, W.M. Yang, Development of 1D model for the analysis of heat transport in cylindrical micro combustors, Appl. Therm. Eng. 29 (2009) 1854–1863.
[22] S.K. Som, U. Rana, Wall heat recirculation and exergy preservation in flow through a small tube with thin heat source, Int. Commun. Heat Mass Transf. 64 (2015) 1–6.
[23] J.L. Wan, A.W. Fan, H. Yao, W. Liu, Effect of thermal conductivity of solid wall on combustion efficiency of a micro-combustor with cavities, Energy Convers. Manage. 96 (2015) 605–612.
[24] C.Y. Hsueh, H.S. Chu, W.M. Yan, G.C. Leu, J.I. Tsai, Three-dimensional analysis of a plate methanol steam micro-reformer and a methanol catalytic combustor with different flow channel designs, Int. J. Hydrogen Energy 36 (2011) 13575–13586.
[25] A.D. Benedetto, V.D. Sarli, G. Russo, Effect of geometry on the thermal behavior of catalytic micro-combustors, Catal. Today 155 (2010) 116–122.
[26] Y. Wang, Z.J. Zhou, W.J. Yang, J.H. Zhou, J.Z. Liu, Z.H. Wang, Instability of flame in micro-combustor under different external thermal environment, Exp. Therm. Fluid Sci. 35 (2011) 1451–1457.
[27] A.D. Stazio, C.C.G. Dayma, P. Dagaut, Combustion in micro-channels with a controlled temperature gradient, Exp. Therm. Fluid Sci. 73 (2016) 79–86.
[28] J. Li, Y. Wang, J. Chen, J. Shi, X. Liu, Experimental study on standing wave regimes of premixed H_2–air combustion in planar micro-combustors partially filled with porous medium, Fuel 167 (2016) 98–105.
[29] V. Vijayan, A.K. Gupta, Combustion and heat transfer at meso-scale with thermal recuperation, Appl. Energy 87 (2010) 2628–2639.
[30] G. Bagheri, S.E. Hosseini, Impacts of inner/outer reactor heat recirculation on the characteristic of micro-scale combustion system, Energy Convers. Manage. 105 (2015) 45–53.
[31] Y. Lei, W. Chen, J. Lei, Combustion and direct energy conversion inside a micro-combustor, Appl. Therm. Eng. 100 (2016) 348–355.
[32] V. Vijayan, A.K. Gupta, Flame dynamics of a meso-scale heat recirculating combustor, Appl. Energy 87 (2010) 3718–3728.
[33] K.S. Kedia, A.F. Ghoniem, The anchoring mechanism of a bluff-body stabilized laminar premixed flame, Combust. Flame 161 (2014) 2327–2339.
[34] J. Li, Q. Li, Y. Wang, Z. Guo, X. Liu, Fundamental flame characteristics of premixed H_2–air combustion in a planar porous micro-combustor, Chem. Eng. J. 283 (2016) 1187–1196.
[35] D. Zhao, L. Li, Effect of choked outlet on transient energy growth analysis of a thermoacoustic system, Appl. Energy 160 (2015) 503–510.
[36] D. Zhao, S. Li, Numerical Investigation of the effect of distributed heat sources on heat-to-sound conversion in a T-shaped thermoacoustic system, Appl. Energy 144 (2015) 204–213.
[37] J.Q. E, W. Zuo, H.J. Liu, Q.G. Peng, Field synergy analysis of the micro-cylindrical combustor with a step, Appl. Therm. Eng. 93 (2016) 83–89.
[38] W. Zuo, J.Q. E, X.L. Liu, Q.G. Peng, Y.W. Deng, H. Zhu, Orthogonal experimental design and fuzzy grey relational analysis for emitter efficiency of the micro-cylindrical combustor with a step, Appl. Therm. Eng. 103 (2016) 945–951.
[39] G. Bagheri, S.E. Hosseini, M.A. Wahid, Effects of bluff body shape on the flame stability in premixed micro-combustion of hydrogen-air mixture, Appl. Therm. Eng. 67 (2014) 266–272.
[40] M. Baigmohammadi, S.S. Sadeghi, S. Tabejamaat, J. Zarvandi, Numerical study of the effects of wire insertion on CH4(methane)/AIR pre-mixed flame in a micro combustor, Energy 54 (2013) 271–284.
[41] W.M. Yang, K.J. Chua, J.F. Pan, D.Y. Jiang, H. An, Development of micro-thermophotovoltaic power generator with heat recuperation, Energy Convers. Manage. 78 (2014) 81–87.
[42] J.T. Niu, J.Y. Ran, L.Y. Li, X.S. Du, R.R. Wang, M.C. Ran, Effects of trapezoidal bluff bodies on blow out limit of methane/air combustion in a micro-channel, Appl. Therm. Eng. 95 (2016) 454–461.

[43] B.J. Lee, C.S. Yoo, H.G. Im, Dynamics of bluff-body-stabilized premixed hydrogen/air flames in a narrow channel, Combust. Flame 162 (2015) 2602–2609.
[44] A.W. Fan, J.L. Wan, K. Maruta, Interactions between heat transfer, flow field and flame stabilization in a micro-combustor with a bluff body, Int. J. Heat Mass Transf. 66 (2013) 72–79.
[45] W. Yang, A.W. Fan, J.L. Wan, W. Liu, Effect of external surface emissivity on flame-splitting limit in a micro cavity-combustor, Appl. Therm. Eng. 83 (2015) 8–15.
[46] J.L. Wan, A.W. Fan, Y. Liu, H. Yao, W. Liu, X.L. Gou, D.Q. Zhao, Experimental investigation and numerical analysis on flame stabilization of CH_4/air mixture in a mesoscale channel with wall cavities, Combust. Flame 162 (2015) 1035–1045.
[47] J.Y. Ran, L.Y. Li, X.S. Du, R.R. Wang, W.L. Pan, W.M. Tang, Numerical investigations on characteristics of methane catalytic combustion in micro-channels with a concave or convex wall cavity, Energy Convers. Manage. 97 (2015) 188–195.
[48] J. Li, Y.T. Wang, J.R. Shi, X.L. Liu, Dynamic behaviors of premixed hydrogen–air flames in a planar micro-combustor filled with porous medium, Fuel 145 (2015) 70–78.
[49] J.S. Hua, M. Wu, K. Kumar, Numerical simulation of the combustion of hydrogen–air mixture in micro-scaled chambers. Part I: fundamental study, Chem. Eng. Sci. 60 (2005) 3497–3506.
[50] J.F. Pan, D. Wu, Y.X. Liu, H.F. Zhang, A.K. Tang, H. Xue, Hydrogen/oxygen premixed combustion characteristics in micro porous media combustor, Appl. Energy 160 (2015) 802–807.
[51] S.Y. Jejurkar, D.P. Mishra, Numerical characterization of a premixed flame based annular micro combustor, Int. J. Hydrogen Energy 35 (2010) 9755–9766.
[52] D.Y. Jiang, W.M. Yang, A.K. Tang, Development of a high-temperature and high-uniformity micro planar combustor for thermophotovoltaics application, Energy Convers. Manage. 103 (2015) 359–365.
[53] Q.B. Lu, J.F. Pan, S. Hu, A.K. Tang, X. Shao, Hetero-/homogeneous combustion of premixed hydrogen-oxygen mixture in a micro-reactor with catalyst segmentation, Int. J. Hydrogen Energy 41 (2016) 12387–12396.
[54] A.K. Tang, J.F. Pan, W.M. Yang, Y.M. Xu, Z.Y. Hou, Numerical study of premixed hydrogen/air combustion in a micro planar combustor with parallel separating plates, Int. J. Hydrogen Energy 40 (2015) 2396–2403.
[55] Y. Su, Q. Cheng, J.L. Song, M.T. Si, Numerical study on a multiple-channel micro combustor for a micro-thermophotovoltaic system, Energy Convers. Manage. 120 (2016) 197–205.
[56] L. Ziani, A. Chaker, Ambient pressure effect on non-premixed turbulent combustion of CH_4–H_2 mixture, Int. J. Hydrogen Energy 41 (27) (2016) 11842–11847.
[57] Y. Liu, J.Y. Zhang, A.W. Fan, J.L. Wan, H. Yao, W. Liu, Numerical investigation of CH_4/O_2 mixing in Y-shaped mesoscale combustors with/without porous media, Chem. Eng. Process. 79 (2014) 7–13.
[58] W.H. Kim, T.S. Park, Effects of noncircular air holes on reacting flow characteristics in a micro can combustor with a seven-hole baffle, Appl. Therm. Eng. 100 (2016) 378–391.
[59] W.D. Wang, CFD mixing analysis of vortex generator jets injected into confined crossflow in rectangular duct, J. Propul. Technol. 19 (2) (1998) 58–62.
[60] J.C. Kurnia, A.P. Sasmito, E. Birgersson, T. Shamim, A.S. Mujumdar, Evaluation of mass transport performance in heterogeneous gaseous in-plane spiral reactors with various cross-section geometries at fixed cross-section area, Chem. Eng. Process. 82 (2014) 101–111.